The effect of stoichiometry on vortex flame interactions

John B. Bell[a], Nancy J. Brown[a], Marcus S. Day[a],
Michael Frenklach[a,b], Joseph F. Grcar[c] and Shaheen R. Tonse[a]

[a] Lawrence Berkeley National Laboratory, Berkeley, CA
[b] Mechanical Engineering Department, UC Berkeley, Berkeley, CA
[c] Sandia National Laboratories, Livermore, CA

Abstract

The interaction of a vortex pair with a premixed flame serves as an important prototype for premixed turbulent combustion. In this study, we investigate the interaction of a counter-rotating vortex pair with an initially flat premixed methane flame. We focus on characterizing the mechanical nature of the flame-vortex interaction and on the features of the interaction strongly affected by fuel equivalence ratio, ϕ. We compare computational solutions obtained using a time-dependent, two-dimensional adaptive low Mach number combustion algorithm that incorporates GRI-Mech 1.2 for the chemistry, thermodynamics and transport of the chemical species. We find that the circulation around the vortex scours gas from the preheat zone in front of the flame, making the interaction extremely sensitive to equivalence ratio. For cases with $\phi \approx 1$, the peak mole fraction of CH across the flame is relatively insensitive to the vortex whereas for richer flames we observe a substantial and rapid decline in the peak CH mole fraction, commencing early in the flame-vortex interaction. The peak concentration of HCO is found to correlate, in both space and time, with the peak heat release across a broad range of equivalence ratios. The model also predicts a measurable increase in C_2H_2 as a result of interaction with the vortex, and a marked increase in the low temperature chemistry activity.

Introduction

Turbulence affects the process of methane combustion through a wide variety of mechanisms. Traditional approaches, based on asymptotic analysis, show that velocity-induced tangential strain at the flame surface, can dramatically enhance or suppress combustion activity in the flame zone depending on Lewis number. These effects have been studied using results from simple, steady flat-flame counterflow experiments (see [1–5]). As discussed in the review by Peters [6], this type of information can readily be incorporated into engineering models through the flamelet concept.

Research aimed at understanding transient effects in turbulent flows has led investigators to study the interaction of a single vortical structure with a premixed flame. These flows offer advantages of being more repeatable and more amenable to analysis and experimental diagnostics than fully developed turbulent flow. Such studies typically consider either a planar vortex pair (for example, see [7–11]), or an axisymmetric toroidal vortex (for example, see [12–19]). Vortex-driven flame quenching has been studied computationally using both single-step [20] and two-step [21] reaction mechanisms. The performance of certain flame markers in the presence of time-dependent vortical perturbations has been assessed in simulations using skeletal C_1 methane chemistry [7, 22] and more complete description of C_1 and C_2 chemistry [23].

While most of the experimental data on methane flame quenching and combustion markers focuses on lean flames, Nguyen and Paul [8] consider a rich methane flame. Their results are particularly interesting for several reasons. First, they predict dramatic changes in species concentrations, particularly CH and OH, that are not predicted by counterflow flame simulations [2]. This suggests that a flamelet model based solely on flat flame data may be inadequate for transient flow field interactions. Second, the limited number of computational studies available for modeling rich multidimensional vortex flame interactions yield results that are somewhat inconsistent with experiment. For example, Najm *et al.* [23] computed a flow problem similar to the Nguyen and Paul experiment. They used the GRI-Mech 1.2 [24] reaction mechanism, and a smaller, faster vortex with less nitrogen dilution; however, their simulations fail to reproduce several key features observed in the experiment.

In this paper, we study in detail the interaction of a vortex with premixed N_2-diluted methane flames having equivalence ratios in the range $\phi = 0.76$–1.28. The vortex we impose matches the strength, core separation and speed of that observed in the Nguyen and Paul experiment. (Although our configuration is close to the actual experimental conditions, we use a flat flame whereas the experimental flame is a V-flame.) We carry out these studies by numerical simulation using a parallel, adaptive low Mach number combustion algorithm developed by Day and Bell [25]. All of the computations use chemistry, transport and thermodynamic databases specified in GRI-Mech 1.2. Our results match the CH behavior

reported in Nguyen and Paul's experiment. In addition we observe that the flame's response to the vortex is a strong function of the inlet flow equivalence ratio. We find that mole fraction of HCO correlates, in both position and time, with the heat release of the methane flame. Finally, we find that in spite of the agreement in CH profiles, our simulations do not reproduce the experimentally observed behavior of OH.

Numerical Model

Our computational approach uses a hierarchical adaptive mesh refinement (AMR) algorithm based on an approximate projection formulation for integrating the momentum equations. The projection algorithm is coupled to conservation equations for chemical species and enthalpy. The single-grid algorithm is implemented in a structured uniform grid setting, and incorporated into an AMR framework that employs a recursive time-stepping procedure over refinement levels. We sketch the model and numerical implementation below; the reader is referred to [25] for details.

Our model is based on a modified form of the low Mach number combustion model introduced by Rehm and Baum [26], subsequently derived from low Mach number asymptotic analysis by Majda and Sethian [27]. Here, the pressure is decomposed as $p(x,t) = p_0 + \pi(x,t)$, where p_0 is the thermodynamic pressure and π is a perturbational pressure that is second order in the Mach number. The original derivation of these equations treats the evolution of momentum, temperature and species subject to a divergence constraint on the velocity field. For numerical purposes we have replaced the temperature evolution equation with a conservation equation for enthalpy. We consider a gaseous mixture, ignoring Soret and Dufour effects, body forces and radiative heat transfer, and assume a mixture model for species diffusion [28] [29]. For an unconfined domain, we can then write

$$\frac{\partial \rho U}{\partial t} + \nabla \cdot \rho UU = -\nabla \pi + \nabla \cdot \tau, \tag{1}$$

$$\frac{\partial \rho Y_m}{\partial t} + \nabla \cdot U \rho Y_m = \nabla \cdot \rho \mathcal{D}_m \nabla Y_m - \dot{\omega}_m, \tag{2}$$

$$\frac{\partial \rho h}{\partial t} + \nabla \cdot U \rho h = \nabla \cdot \frac{\lambda}{c_{p,mix}} \nabla h + \sum_m \nabla \cdot h_m (\rho \mathcal{D}_m - \frac{\lambda}{c_{p,mix}}) \nabla Y_m \tag{3}$$

where ρ is the density, U is the velocity, Y_m is the mass fraction of species m ($\sum_m Y_m = 1$), h is the enthalpy of the gas mixture, T is the temperature, and $\dot{\omega}_m$ is the net destruction rate for ρY_m due to chemical reactions. The stress tensor is given by

$$\tau = \mu \left(\frac{\partial U_i}{\partial x_j} + \frac{\partial U_j}{\partial x_i} - \frac{2}{3} \delta_{ij} \nabla \cdot U \right)$$

where $\mu(Y_m, T)$ is the viscosity. Also, $\mathcal{D}_m$ are the species mixture-averaged diffusion coefficients [28], λ is the thermal conductivity, $c_{p,mix}$ is the specific heat of the mixture and $h_m(T)$ is the enthalpy of species m. These evolution equations are supplemented by an equation of state:

$$p_0 = \rho R_{mix} T = \rho \mathcal{R} T \sum_m \frac{Y_m}{W_m} \tag{4}$$

where W_m is the molecular weight of species m, and by a relationship between enthalpy, species and temperature:

$$h = \sum_m Y_m h_m(T) \quad . \tag{5}$$

The evolution specified by (1-3) is subject to the constraint that

$$\begin{aligned} \nabla \cdot U \;\; = \;\; & \frac{1}{\rho c_p T} \left(\nabla \cdot \lambda \nabla T + \sum_m \rho \mathcal{D}_m \nabla Y_m \cdot \nabla h_m \right) + \\ & + \frac{1}{\rho} \sum_m \frac{W}{W_m} \nabla \cdot \rho \mathcal{D}_m \nabla Y_m \;\; + \frac{1}{\rho} \sum_m \left(\frac{h_m(T)}{c_{p,mix} T} - \frac{W}{W_m} \right) \dot{\omega}_m \equiv S \end{aligned} \tag{6}$$

where $W = (\sum_m Y_m / W_m)^{-1}$ and $c_{p,mix} = \sum_m Y_m dh_m/dT$. This constraint is obtained by differentiating the equation of state along particle paths and replacing the Lagrangian derivatives by expressions obtained from (2, 3, 5).

The single-grid scheme that forms the basis for our adaptive algorithm couples an implicit treatment of differential diffusion to a symmetric operator-split time-advancement of chemical reactions. The resulting algorithm is convergent to second order in Δt. We first describe briefly the single grid integration scheme and then indicate how the methodology is incorporated into an adaptive mesh algorithm.

The projection formulation for advancing the momentum equations subject to (6) is based on a fractional step algorithm presented by Almgren, *et al.* [30] which was extended to low Mach number flows by Pember *et al.* [31]. First, equations (1–3) are advanced in time using a lagged pressure gradient without specific regard to the divergence constraint. This step incorporates a high-resolution Godunov scheme for convective terms and a time-centered Crank-Nicolson discretization for diffusion. Because the mixture diffusion coefficients depend on both temperature and composition, we adopt a sequential, predictor-corrector scheme to guarantee second-order treatment of nonlinear diffusion effects. The chemistry is advanced in a symmetric time-split fashion using implicit methods in VODE [32]. The velocity, U^*, resulting from this advection/diffusion/chemistry step fails to satisfy the constraint (6). In the projection, we solve the variable coefficient Poisson equation, $\nabla \cdot \frac{1}{\rho} \nabla \chi = \nabla \cdot U^* - S$ for χ. The new-time velocity, U^{new}, is then computed from

$$U^{new} = U^* - \frac{1}{\rho} \nabla \chi$$

so that $\nabla \cdot U^{new} = S$. Here, χ represents a time-centered correction to the perturbational pressure. The Godunov procedure for convective terms is explicit so the algorithm requires a CFL-type time-step restriction. Since the advective time scale is typically larger than the chemical time scales this does not appear to be a serious disadvantage for time dependent simulations.

The algorithm has a number of desirable properties. The overall method is second-order accurate and discretely conserves species mass density and enthalpy. Temperature appears only as an auxiliary quantity in the algorithm; the final temperature resulting from the update is obtained by inverting (5). Furthermore, the algorithm satisfies a free-stream preservation property—species that have an initial uniform mass distribution and do not participate in reactions remain uniform.

We note that because of the fractional step nature of the overall approach it is impossible to numerically conserve species and enthalpy while satisfying the equation of state (4). Although we discretely conserve both species and energy the evolution of these quantities does not satisfy the equation of state (with T determined from (5)). In order to prevent the algorithm from drifting too far off the equation of state, we add a correction term

$$f \, \frac{c_{p,mix} - R}{\Delta t \; c_{p,mix} \hat{p}} \, (\hat{p} - p_0) \tag{7}$$

to the right hand side of the constraint equation (6) where $\hat{p}$ is the thermodynamic pressure, defined by (4), and $f < 1$ is a numerical damping factor. This additional term serves to damp the system back onto the ambient equation of state if the solution drifts off that constraint.

The extension of the above algorithm to adaptive mesh refinement is based on a hierarchical refinement strategy. Our methodology uses a sequence of nested grids with successively finer spacing in time and space. Fine grids are formed by uniformly dividing coarse cells by a refinement ratio, r, in each direction. Increasingly finer grids are recursively embedded in coarse grids until the solution is adequately resolved. An error estimation procedure is used to identify where refinement is needed and grid generation procedures dynamically create or remove rectangular fine grid patches as requirements change.

The adaptive integration algorithm advances grids at different levels using time steps appropriate to that level, based on CFL considerations. The integration algorithm is a recursive procedure in which we first integrate the coarse grid. We then integrate the fine grid multiple steps until it reaches the same time as the coarse grid. Finally, we sychronize the levels to enforce conservation and a set of elliptic matching conditions (see Day and Bell [25]).

The adaptive refinement algorithm preserves the key features of the single grid algorithm. In particular, the overall algorithm is second-order accurate, conserves both species and enthalpy, and maintains the free-stream preservation property described above. The

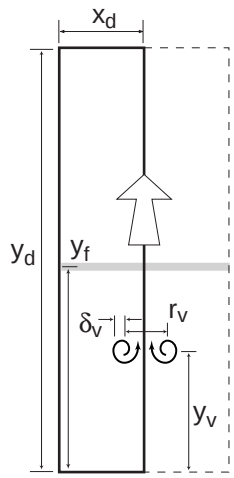

Fig. 1 - Schematic of the premixed methane flame-vortex problem. The shaded line represents the position of the flame, and the swirl lines represent the initial vortex. We impose symmetry along the sides of the 0.8×4.0 cm domain to avoid modeling the dotted region.

methodology has been implemented for distributed memory parallel processors using the BOXLIB class libraries described by Rendleman *et al.* [33].

Results

We conducted a detailed study of a counter-rotating pair of vortices interacting with 32.5% N_2-diluted premixed methane-air flames. We focus the discussion on two aspects of the results. First, we are interested in characterizing the mechanical nature of the flame-vortex interaction. Second, we want to understand how this behavior affects the combustion process as a function of flame stoichiometry.

The computational study approximates the experimental conditions of Nguyen and Paul. Following Najm *et al.*, we approximate the V-flame experiment as a flat premixed flame oriented normal to the inlet flow, and superimpose a velocity field due to a periodic array of counter-rotating vortex pairs with Gaussian cores $\delta_v = 2.25$ mm wide and centers $r_v = 0.25$ cm apart. The vortex pair propagates upward with a self-induced velocity of 110 cm/s. These parameters produce a vortex pair with the same width and propagation speed as reported for the vortex pair in the Nguyen and Paul experiment. We numerically evolve only the left vortex as indicated in Fig 1. Our base computational domain is $x_d = 8$ mm wide, and $y_d = 4$ cm high, with the boundary along the right side corresponding to the vortex centerline. The periodic configuration results from symmetry boundary conditions imposed on the sides of the domain. Reactants flow in the bottom, and combustion products exit the top.

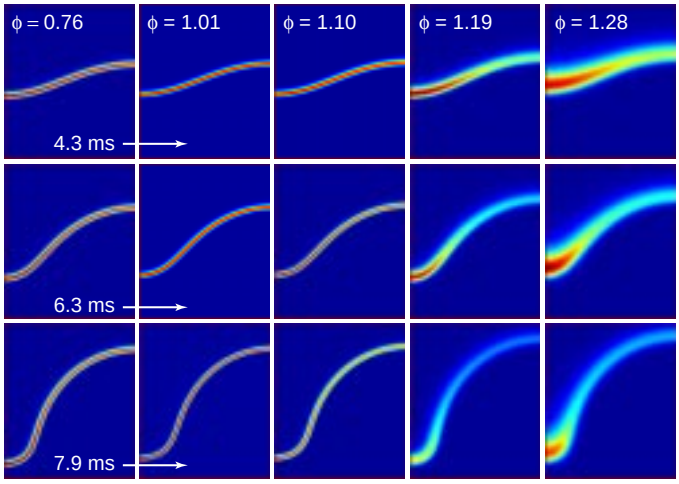

Fig. 2 - CH mole fraction. In each column, the three frames correspond approximately to 4.3, 6.3 and 7.9 ms simulation time from the initial conditions (see Fig 1). The color scale in each column is normalized to peak values of $X_{\mathrm{CH}} = 0.23$, 7.76, 10.8, 3.66, 0.30×10^{-7}, respectively. The frames represent 8×9.5 mm subregions of the domain near the flame surface.

We position the initial premixed flame so that the peak mole fraction of HCO occurs at $y_f = 2$ cm (see Fig 1). Cell-centered values are initialized using cell-averages of a refined PREMIX [34] solution, and a superimposed vortex. The vortex is initialized halfway between the inlet and flame. We cover the entire domain with a uniform coarse mesh ($\Delta x = 250\mu$m), and then place up to two refined grid levels, each with Δx decreased by a factor of two, to resolve the flame zone. The resulting resolution is equivalent to a 128×640 uniform grid calculation with $\Delta x = 62.5\mu$m. To determine whether image vortices introduced by the symmetry boundary conditions significantly impact these results, we also performed calculations on larger domains. Results on the smaller domain depicted in Fig 1 are insensitive to the domain size for the first 10 ms of simulation time; for longer times there are noticeable edge effects. Where we report longer time results, we use data computed on domains sufficiently large that the edge effects are not manifest.

For the simulations, we chose five inlet stoichiometries, ϕ equal 0.76, 1.01, 1.10, 1.19, and 1.28. In Fig 2, we present snapshots depicting the mole fraction of CH for each stoichiometry. At 7.9 ms, the vortex center has traveled 80% of the distance initially separating the flame and vortex, and has interacted with the flame significantly. The extent of the simulated decline in the CH signal is dependent on the overall flame stoichiometry. There is no noticeable change in the peak value of CH along the flame surface for $\phi = 0.76$, and only a very small decline for the $\phi = 1.01$ case. At $\phi = 1.10$, the decline becomes pronounced, and it steepens with further increases in the equivalence ratio.

The case $\phi = 1.19$ corresponds to the stoichiometry (and nitrogen dilution) used in

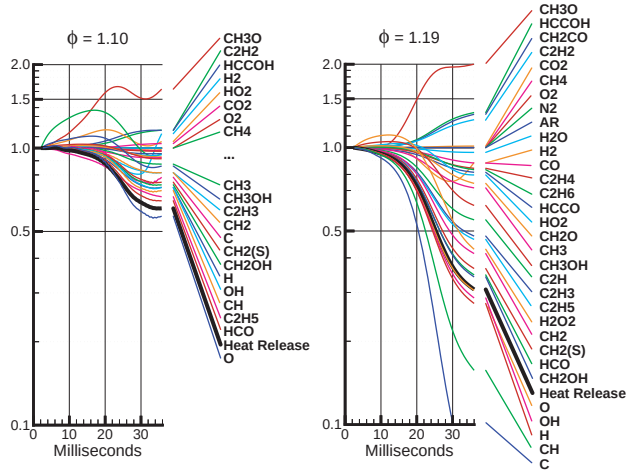

Fig. 3 - Time history of the peak values of molar concentration, normalized to their respective values at $t = 2$ ms. Normalization is made at this later time to avoid initial transients as the PREMIX solution adjusts to the AMR grid. Note these data are taken from simulations on very large 1.2×5.6 cm domains to avoid edge effects at later times in the flame vortex interaction.

Nguyen and Paul's experiment. They observe a two- to threefold decrease in the averaged CH signal before it abruptly disappears. The loss of signal occurs throughout the flame sheet wrapped around the vortex, and occurs about 7 ms after the vortices first begin to distort the flame. Examination of our numerical results indicate that CH concentration for this case exhibits a similar rapid decline leading eventually to a nearly tenfold decrease. This simulated rate of decrease is consistent with the PLIF signal descending to its noise level in the time interval observed. Moreover, Fig 2 shows that the simulated CH concentration declines precisely in the region identified by Nguyen and Paul.

A more detailed examination of the computational results indicates that there is actually a qualitative shift in the behavior of CH between $\phi = 1.10$ and $\phi = 1.19$. In Fig 3 we show time histories of the peak molar concentration of each species along the right boundary of the computational domain for the two cases. In the rich cases ($\phi \geq 1.19$), the peak in CH declines more rapidly than the peak heat release; the opposite is true in the lean cases ($\phi \leq 1.10$).

The change in CH behavior is one example of how the vortex modifies the flame. Asymptotic analysis suggests that stretched and strained flames exhibit a reduction in combustion heat release [35, p. 418]. We find the circulation around the vortex scours gas from the preheat zone in front of the flame. During early times, the gases swept away are replaced with the inlet fuel mixture. The scoured gases become entrained in the rotational flow, and are re-injected later by the vortex. The early effects of vortex scouring are related closely to local Lewis numbers and are extremely sensitive to the equivalence ratio. Fig 4 illustrates the

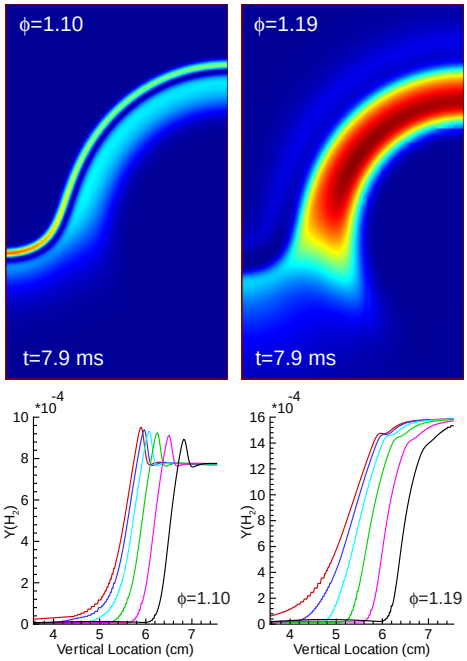

Fig. 4 - H_2 diffusion flux $\left|\rho D_{H_2} \nabla Y_{H_2}\right|$ for $\phi = 1.10, 1.19$ at 7.9 ms. Also, H_2 mass fraction along vortex centerline (right domain boundary) at selected times in the range $0 \leq t \leq 7.9$ ms. The broader Y_{H_2} profile for $\phi = 1.19$ is scoured out of the region in front of the flame by the approaching vortex, enhancing diffusive transport. The narrow Y_{H_2} profile for the $\phi = 1.10$ case is not similarly affected.

early effects of vortex scouring on the H_2 profile for the $\phi = 1.10$ and $\phi = 1.19$ cases. In the richer case, there is a substantial amount of H_2 in front of the the unperturbed flame. Later, the vortex motion has swept away much of the H_2 gas from the region in front of the flame. In the images of H_2 diffusion flux, each normalized to peak values over the entire evolution for their respective inlet stoichiometry, we observe a dramatic increase in the $\phi = 1.19$ case. This enhanced diffusion serves to replenish concentrations that are being swept away by the vortex. The scouring penetration depth into the flame is limited by the gas expansion due to heat release in the main combustion zone, but Fig 4 illustrates that diffusion can couple the vortex to processes well within the flame. In the leaner case there is less excess H_2 to diffuse into the low-temperature region, consequently, the vortex fails to dramatically alter the H_2 mass fraction and diffusion profiles.

This role of vortex scouring can be isolated from the effects of stretch and strain in a one dimensional model. We have modeled the effect of the vortex sweeping away material in front of the flame and replenishing it with inlet gases by a source term that draws material from the cold region of the one-dimensional flame and replaces it with the inlet mixture on a time scale comparable to the vortex motion. Computational experiments with this simple

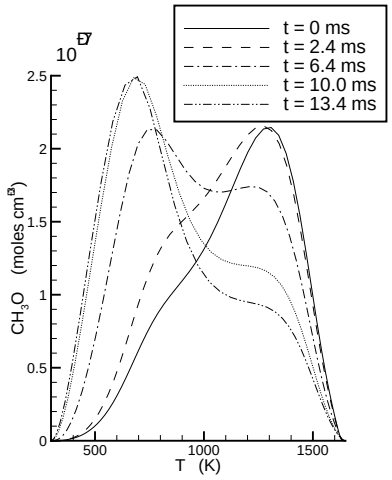

Fig. 5 - CH_3O profiles along the vortex centerline for $\phi = 1.19$. During the flame-vortex interaction, there is a marked enhancement of CH_3O concentration in low temperature regions.

model show a dramatic decline in CH for the rich $\phi = 1.19$ case and essentially no change in CH for the lean $\phi = 1.10$ case. The one-dimensional computations do not contain the effects of stretch and strain that complicate the two-dimensional flows. Thus, the behavior of CH in the one dimensional model indicates that vortex scouring is responsible for the dramatic decline of CH in the rich case relative to the decline in heat release.

Although the notion of vortex scouring in combination with effects due to stretch and strain describe the mechanisms by which the vortex modulates the flame, the net result of this modification can be quite complex. It is compelling to conjecture that the dominant effect in the rich case is the removal of H_2 from the front of the flame. However, tests of this hypothesis in the one-dimensional scouring code show that this is not the case. In general, the effects of vortex scouring depend on preferential diffusion effects in competition with reactions and on the specific reaction pathways that are dominant in a given region of the flame.

The flame structures were also analyzed using reaction path analysis. The reaction pathways are those that one would expect, namely the C_1 pathway to formyl radical, and an enhancement of the C_2 pathways with increasing equivalence ratio. The sensitivity analysis showed the dominance of reactions that are most important in controlling the size of the radical pool, and in many cases the sensitivities showed self-similarity indicating that only a few variables control the state of the system. In agreement with Najm *et al.*, we find that the formyl radical, HCO, is a reliable marker for heat release. The numerical results presented in Fig 3 as well as similar analyses for other stoichiometries confirm this for flames interacting with vortices. The dramatic decrease of CH in rich flames is linked to the decrease of H

atom concentrations and triplet methylene, and decreases in important production rates. Interestingly, some species increase in concentration in low temperature zones. For example, for ϕ =1.19, the species CH_3O, C_2H_2, HO_2, CH_3, HCCOH, CH_2CO,and CO_2 increase. The most dramatic example of this occurs for CH_3O, as shown in Fig 5. We note a shift of the peak concentration to lower temperatures as the vortex couples more strongly with the flame. Sensitivity analysis indicates a linkage between the increase in CH_3O and the decline in CH. Another noteworthy feature is the increase in the C_2H_2 concentration which occurs as a result of the flame-vortex interactions. This prediction is potentially significant for soot modeling.

Conclusions

Numerical simulations of vortex flame interactions have revealed a strong dependence of CH behavior on equivalence ratio. Analysis of this behavior has shown that the vortex not only stretches and strains the flame, it also scours material from the cold region in front of the flame and replenishes the flow with inlet gases at early time. This scouring effect produces the dramatic decline in CH observed experimentally by Nguyen and Paul. The model predicts a measurable increase in C_2H_2 as a result of the vortex, and a marked increase in the low-temperature chemistry activity.

The model fails to reproduce the enhancement of OH observed by Nguyen and Paul. One possibility is that, with our current limited knowledge of the low-temperature chemistry, some unknown chemistry or imprecise knowledge of thermochemistry might lead to the experimentally observed rise in OH signal. However, precisely because this chemistry is so poorly known, such specific speculations are unwarranted at this time. The approximation of the V-flame by a flat flame and enhanced mixing not represented in the two dimensional flow model are other possible sources of discrepancy.

Acknowledgments

The work of JB and MD was supported by the Applied Mathematics Program of the DOE Office of Mathematics, Information, and Computational Sciences, and that of NJB, MF,and SRT by the Laboratory Directed Research and Development Program of Lawrence Berkeley National Laboratory under the U.S. Department of Energy under contract No. DE-AC03-76SF00098. JG's work was supported by Sandia National Laboratories, a multiprogram laboratory operated by Sandia Corporation, a Lockheed Martin Company, for the United States Department of Energy under Contract DE-AC04-94AL85000.

References

[1] Egolfopoulos, F., *Twenty-Fifth Symposium (International) on Combustion*, The Combustion Institute, Pittsburgh, PA, 1994, pp. 1365–1373.

[2] Kee, R. J., Miller, J. A., Evans, G. H., and Dixon-Lewis, G., *Twenty-Second Symposium (International) on Combustion*, The Combustion Institute, Pittsburgh, PA, 1988, pp. 1479–1494.

[3] Law, C. K., *Twenty-Second Symposium (International) on Combustion*, The Combustion Institute, Pittsburgh, PA, 1988, pp. 1381–1402.

[4] Petrov, C. and Ghoniem, A., *Combust. Flame*, 102:401–417 (1995).

[5] Rogg, B., *Combust. Flame*, 73:45–46 (1988).

[6] Peters, N., *Twenty-First Symposium (International) on Combustion*, The Combustion Institute, Pittsburgh, PA, 1986, pp. 1231–1250.

[7] Najm, H. N., Paul, P. P., Mueller, C. J., and Wyckoff, P. S., *Combust. Flame*, 113:312–332 (1998).

[8] Nguyen, Q.-V. and Paul, P. H., *Twenty-Sixth Symposium (International) on Combustion*, The Combustion Institute, Pittsburgh, PA, 1996, pp. 357–364.

[9] Paul, P. H. and Najm, H. N., *Twenty-Seventh Symposium (International) on Combustion*, The Combustion Institute, Pittsburgh, PA, 1998, pp. 43–50.

[10] Samaniego, J.-M., *Annual Research Briefs*, Center for Turbulence Research, Stanford, California, 1993, Stanford University / NASA Ames Research Center.

[11] Samaniego, J.-M. and Mantel, T., *Combust. Flame*, 118:537–556 (1999).

[12] Driscoll, J. F., Sutkus, D. J., Roberts, W. L., Post, M. E., and Goss, L. P., *Combust. Sci. Technol.*, 96:213 (1994).

[13] Mueller, C. J., Driscoll, J. F., Reuss, D. L., and Drake, M. C., *Twenty-Sixth Symposium (International) on Combustion*, The Combustion Institute, Pittsburgh, PA, 1996, pp. 347–355.

[14] Mueller, C. J., Driscoll, J. F., Reuss, D. L., Drake, M. C., and Rosalik, M. E., *Combust. Flame*, 112(3):342–358 (1998).

[15] Mueller, C. J., Driscoll, J. F., Sutkus, D. J., Roberts, W. L., Drake, M. C., and Smooke, M. D., *Combust. Flame*, 100:323–331 (1995).

[16] Roberts, W. L. and Driscoll, J. F., *Combust. Flame*, 87:245 (1991).

[17] Roberts, W. L., Driscoll, J. F., Drake, M. C., and Goss, L. P., *Combust. Flame*, 98:58–69 (1993).

[18] Roberts, W. L., Driscoll, J. F., Drake, M. C., and Ratcliffe, J. W., *Twenty-Fourth Symposium (International) on Combustion*, The Combustion Institute, Pittsburgh, PA, 1992, p. 169.

[19] Rolon, J. C., Aguerre, F., and Candel, S., *Combust. Flame*, 100:422–429 (1995).

[20] Poinsot, T. J., Veynante, D., and Candel, S. M., *J. Fluid Mech.*, 228:561–606 (1991).

[21] Mantel, T., *Annual Research Briefs*, Center for Turbulence Research, Stanford, California, 1994, Stanford University / NASA Ames Research Center.

[22] Najm, H. N. and Wyckoff, P. S., *Combust. Flame*, 110:92–112 (1997).

[23] Najm, H.N., Knio, O. M.., Paul, P. P., and Wyckoff, P. S., *Combust. Sci. Technol.*, 140:369–403 (1998).

[24] Frenklach, M., Wang, H., Goldenberg, M., Smith, G. P., Golden, D. M., Bowman, C. T., Hanson, R. K., Gardiner, W. C., and Lissianski, V."GRI-Mech—An optimized detailed chemical reaction mechanism for methane combustion," Gas Research Institute Report No. GRI-95/0058, see also http://www.me.berkeley.edu/gri_mech/.

[25] Day, M. S. and Bell, J. B., *Combust. Theory Model*, (1999), submitted.

[26] Rehm, R.G. and Baum, H.R., *N.B.S.J.Res.*, 83:297–308 (1978).

[27] Majda, A. and Sethian, J. A., *Combust. Sci. Tech.*, 42:185–205 (1985).

[28] Kee, R. J., Dixon-Lewis, G., Warnatz, J., Coltrin, M. E., and Miler, J. A."A FORTRAN computer code package for the evaluation of gas-phase multicomponent transport properties," Sandia National Laboratories Report No. SAND86-8246.

[29] Warnatz, J., (Peters, N. and Warnatz, J., editors), *Numerical methods in flame propagation*, Friedr. Viewweg and Sohn, Wiesbaden, 1982.

[30] Almgren, A. S., Bell, J. B., Colella, P., Howell, L. H., and Welcome, M., *J. Comput. Phys.*, 142:1–46 (1998).

[31] Pember, R. B., Howell, L. H., Bell, J. B., Colella, P., Crutchfield, W. Y., Fiveland, W. A., and Jessee, J. P., *Comb. Sci. Tech.*, 140:123–168 (1998).

[32] Brown, P. N., Byrne, G. D., and Hindmarsh, A. C., *SIAM J. Sci. Stat. Comput.*, 10:1038–1051 (1989).

[33] Rendleman, C. A., Beckner, V. E., Lijewski, M., Crutchfield, W. Y., and Bell, J. B., "Parallelization of structured, hierarchical adaptive mesh refinement algorithms," Technical Report LBNL-43154, accepted, Computing and Visualization in Science.

[34] Kee, R. J., Grcar, J. F., Smooke, M. D., and Miller, J. A."A FORTRAN program for modelling steady laminar one-dimensional premixed flames," Sandia National Laboratories Report No. SAND85-8240.

[35] Williams, F. A., *Combustion Theory* (2nd ed), The Benjamin/Cummings Publishing Company, Inc., 1985.